Light Scattering Studies on the Morphology and Deformation Mechanism of Poly(tetramethylene oxide)–Poly(tetramethylene terephthalate) Block Polymer. 2. Rodlike Textures

Chie Sawatari, Masayasu Iida,† and Masaru Matsuo*

Department of Clothing Science, Faculty of Home Economics, Nara Women's University, Nara 630, Japan. *Received April 25, 1983*

ABSTRACT: An interesting phenomenon was found in the formation of rodlike textures in poly(tetramethylene oxide)–poly(tetramethylene terephthalate) block copolymer. Rodlike textures were formed when amorphous films were preheated and stretched. In order to obtain detailed information concerning the rods, the morphology and the deformation were studied by polarizing microscopy and small-angle light scattering. Under polarizing microscopy, the rodlike textures were oriented at a particular angle with respect to the stretching direction and formed networks. The corresponding scattering showed a superposition of a broad four-leaf pattern as lobes and a sharp four-leaf pattern as streaks. Such a relationship has already been observed in drawn films of poly(tetramethylene terephthalate) homopolymer. On the basis of the results observed, a model is proposed to calculate H_v light scattering patterns from the assemblies of the oriented rods forming network units. With a proper choice of parameters associated with the orientations of the rods and of the assemblies, the patterns calculated were in good agreement with the ones observed. This indicates that the sharp streaks are to be attributed as an interparticle interference effect of the rods.

I. Introduction

There is currently considerable interest[1-6] in the fine structure and physical properties of segmented polymers synthesized by combining blocks or segments of two dissimilar homopolymers to form a polymer chain. One component is characterized as a rubbery or soft segment with a relatively low glass transition temperature and the other as a hard segment having a glassy–amorphous or semicrystalline nature. Such copolymers have been made from styrene and isoprene cast from several solvents, and the morphology has been shown to consist of spheres, rods, or sheets of one component dispersed in a continuous matrix of the other.[7-10]

In a previous paper,[11] the morphology and deformation mechanism were studied for a poly(tetramethylene oxide)–poly(tetramethylene terephthalate) block copolymer with a relatively high ratio of soft to hard segments (1:3), using small-angle light scattering and polarizing microscopy. When specimens obtained by solvent casting were formed as thin films several tens of microns in thickness by pouring 0.5% solutions in 1,1,2-trichloroethane into a flat cell at 73 ± 4 °C, the light scattering pattern exhibited a four-leaf clover shape in the undeformed state, the lobes of which were extended in the horizontal direction with elongation. On the other hand, when samples were molded at 200 °C for 10 min at a pressure of 140 kg/cm^2 and were immediately quenched to room temperature, the scattering patterns were of two types. One has maximum intensity at particular azimuthal angles $(2n + 1)\pi/4$ (n = 0–3), which has usually been found in the scattering from the spherulitic textures of crystalline polymers. The other has maximum intensity at $n\pi/2$ (n = 0–3), which was characteristic of poly(tetramethylene terephthalate) homopolymers, as reported by Seymour et al.[5] and Cooper et al.[6]

In this paper, poly(tetramethylene oxide)–poly(tetramethylene terephthalate) with a relatively low concentration of soft rubbery segments was employed in order to study the effect of the ratio of soft to hard segments on the morphology and deformation mechanism discussed in the previous paper.[11] The specimen molded in the previous manner was quenched by being plunged into an ice–water bath. No superstructure was observed under polarizing microscopy. When the specimen was elongated, rodlike textures appeared that were oriented at a particular angle with respect to the stretching direction. The existence of such rodlike textures in this segmented polyether–polyester block copolymer has never been reported, so the main focus of the present work is concentrated on the detailed analysis of the morphology and deformation mechanism of rodlike textures by small-angle light scattering and polarizing microscopy.

II. Experimental Section

Crude pellets of poly(tetramethylene oxide)–poly(tetramethylene terephthalate) were obtained through the courtesy of Katada Institute, Toyo-bo Co., Ltd. This kind of segmented polyether–polyester block copolymer consists of random sequences of soft and hard segments. The soft and hard segments are given by

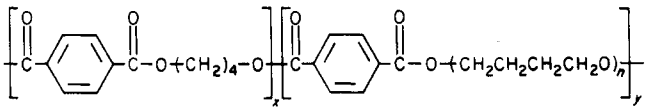

where x and y are averages that depend on the polymerization conditions. The ratio of y to x is 14:1 and 6:1 for the specimens labeled P150B and P70B, respectively. The total molecular weights for both the block copolymers are 40 000–50 000. The crude pellets were treated with ethanol for 30 h in a Soxhlet extractor before use. Following the method of Stein and Mirsa,[12] the extracted pellets for P150B and P70B were sandwiched between Teflon sheets at 235 and 200 °C, respectively, for 10 min at a pressure of 140 kg/cm^2. The molten sample was quenched by being plunged into an ice–water bath. The film thickness for P150B and that for P70B are about 50 μm. The densities of both were measured by a pycnometer, using a carbon tetrachloride–*n*-heptane mixture as the medium.

The films obtained were preheated at several temperatures between 80 and 160 °C for 10 min and stretched to various desired extension ratios. In this process, the formation of rodlike textures was observed by polarizing microscopy and small-angle light scattering.

Light scattering patterns were obtained with a 3-mW He–Ne gas laser as a light source. Diffuse surface scatter was avoided by sandwiching the specimen between microscope cover slides with silicone oil of an appropriate index as an immersion fluid. Polarizing microscopy was performed with a Nikon Optiphot Pol (XTP-11). This made visible structures that were too small to

† Department of Chemistry, Faculty of Science, Nara Women's University.

0024-9297/84/2217-1765$01.50/0

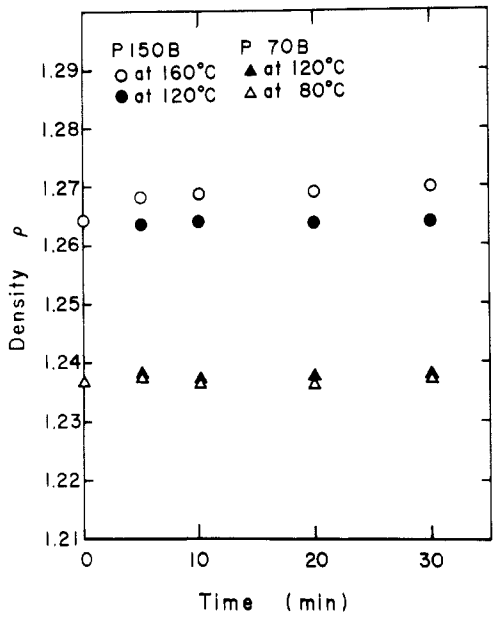

Figure 1. Density vs. annealing time for specimens P150B and P70B annealed at the indicated temperatures.

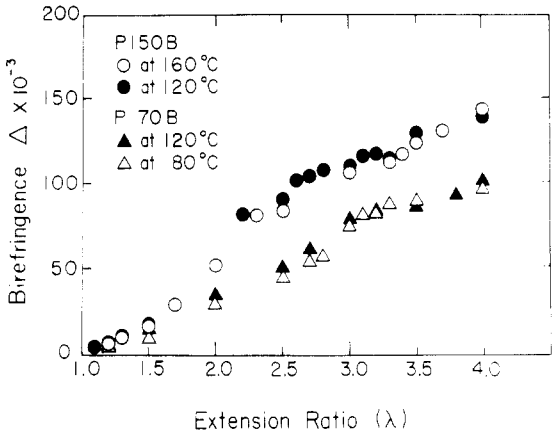

Figure 2. Birefringence vs. extension ratios for specimens P150B and P70B stretched at the indicated temperatures.

be detected by small-angle light scattering.

III. Results and Discussion

Figure 1 shows the density for the specimens P150B and P70B as a function of annealing time at several temperatures between 80 and 160 °C. The density shows an almost constant value, being independent of thermal crystallization except in the case when specimen P150B, stretched at 160 °C, exhibits an increase in the first 5 min and then tends to level off beyond 5 min. This tendency was similar to that for poly(tetramethylene terephthalate) homopolymer,[15] but the increase in density was not pronounced in comparison with that in the case of the homopolymer. As can be seen in Figure 1, it would be expected that both the block copolymers P150B and P70B would crystallize rapidly at temperatures less than 0 °C and the degree of crystallinity is presumably close to the intrinsic maximum value that these copolymers can attain.

The total orientation behavior of hard and soft segments can be determined by measuring the change in birefringence, as shown in Figure 2. The increase in birefringence indicates the preferential orientation of the optical axes, i.e., the molecular chains of soft and hard segments. The degree of birefringence is almost independent of the elongation temperature and is affected only by the concentration ratio of soft to hard segments. That is, the

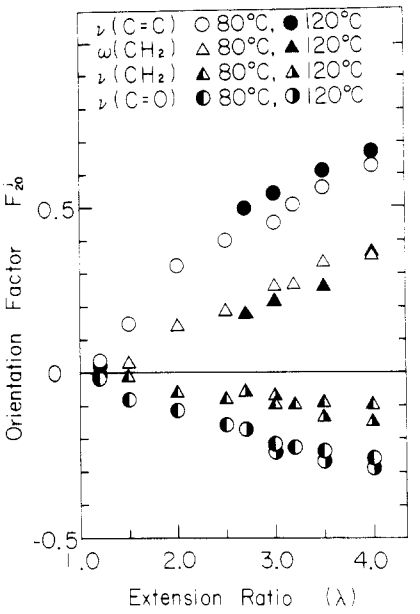

Figure 3. Orientational behavior of soft and hard segments for specimen P70B in terms of the second-order orientation factor of the indicated transition moments.

molecular orientation of P150B with the ratio 1:14, is much more pronounced than that of P70B, with the ratio 1:6, as the elongation ratio increases. It should be noted that this difference is due to the mobility of the molecular chains under stretching. When specimen P150B, with a relatively low concentration of soft rubbery segments, is stretched, the strain increases considerably and does not relax with further increases of λ; this implies a considerable orientation of polymer chains. In contrast, when specimen P70B, with a relatively high concentration of soft segments, is stretched, the strain that occurs during elongation relaxes easily, so that there is a gradual increase in the orientation of the polymer chains. This concept is supported by the fact that poly(tetramethylene terephthalate) exhibited a considerable increase in birefringence over that of specimen P150B.[15]

In order to investigate the orientational difference between soft and hard segments, the orientational behavior of specimen P70B was evaluated in terms of the second-order orientation factor of the transition moment of the jth group as measured by infrared dichroism. The orientation factor is defined by

$$F_{20}^j = \frac{3\langle\cos^2\alpha_j\rangle - 1}{2} = \frac{A_\parallel^j - A_\perp^j}{A_\parallel^j + 2A_\perp^j} \qquad (1)$$

where α_j is the orientation angle of the transition moment of the jth group with respect to the stretching direction and $A_\parallel^j$ and $A_\perp^j$ are optical densities, obtained by the base-line method, at the absorption maximum of polarized light parallel and perpendicular to the stretching direction, respectively. Figure 3 shows the results calculated with eq 1 for specimen P70B stretched up to λ = 4.0. Judging from the structural formula of this segmented polyether–polyester block copolymer, the transition moments of ν(C═C) and ν(C═O), the absorptions of which occur at 1580 and 1690 cm^{-1}, are presumably associated with the orientational behavior of the hard segments, while those of $\omega(CH_2)$ at 1370 cm^{-1} and $\nu(CH_2)$ at 2790 cm^{-1} are associated with the orientation of soft segments. The orientational behavior of the transition moments of ν(C═C) and ν(C═O) shows a monotonic increase in positive and negative orientations of hard segments, respectively. The transition moments of the ν(C═C) stretching vibration of

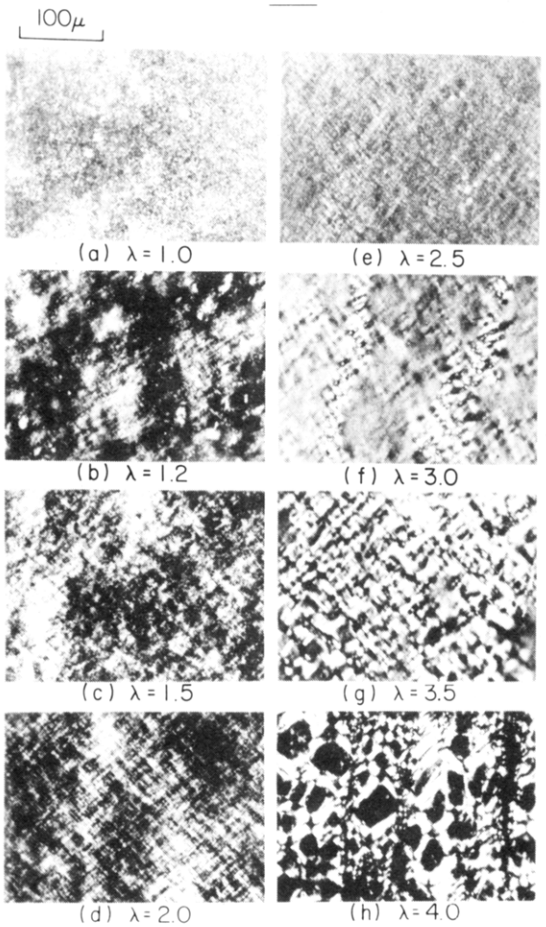

Figure 4. Change in polarized micrographs of specimen P70B stretched at 120 °C.

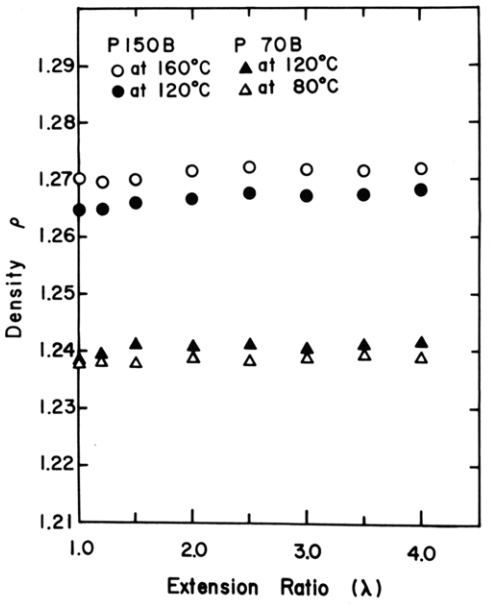

Figure 5. Density vs. elongation ratio for specimens P150B and P70B stretched at the indicated temperatures.

the phenylene ring and ν(C=O) may be assumed to orient parallel and perpendicular to the chain direction, respectively. As for the soft segments, the transition moments of the $\omega(CH_2)$ and $\nu(CH_2)$ bands, wagging and antisymmetric stretching of the CH_2 group, give monotonic positive and negative orientations, respectively. The transition moments of $\omega(CH_2)$ and $\nu(CH_2)$ can be assumed to orient parallel and perpendicular to the chain direction, respectively. On the basis of the above assumption, it may be concluded that the orientation of hard segments is much more pronounced than that of soft segments, while the orientation factor of hard and soft segments is hardly affected by the elongation temperature. This is in good agreement with the change in birefringence in Figure 2. The hard segments show positive orientation even at relatively small elongation, and this tendency is quite different from the behavior observed for drawn films with spherulitic textures by Cooper et al.[6] According to their report,[6] the hard segments showed negative orientation, characterizing deformation of spherulites at relatively small elongation, which changes to positive orientation at higher extension.

In addition, we made polarizing microscopic observations and small-angle light scattering measurements on specimen P70B stretched to the indicated elongation ratios at 120 °C to obtain information on the deformation of the superstructure. Figure 4 shows the polarized micrographs. As can be seen in Figure 4a, no superstructure was observed in this film preheated prior to deformation. This indicates, as discussed already by Stein and Misra,[12] that during crystallization of poly(tetramethylene terephthalate), corresponding to the hard segments, from the glassy state, the nucleation density is very high, which results in a superstructure of very small dimensions that cannot be resolved by the polarizing microscope.

When the specimen was stretched, rodlike textures appeared at draw ratios as low as $\lambda = 1.2$. Photographs b–f seem to suggest a rodlike texture existing in the interior of the specimen. The rods are oriented at nearly 45° with respect to the stretching direction and form networks at elongation ratios less than $\lambda = 3.0$. With further elongation, the networks are disrupted but the rods are still oriented at around 45°. That is, the rods retain the orientational angle of 45°, despite the fact that the molecular chain axes of the soft and hard segments become oriented more and more in the stretching direction, as shown in Figure 3. This interesting behavior is presumably due to the predominant orientation of soft and hard segments within amorphous regions, i.e., the boundaries between the adjacent crystallites.

The network structures are quite similar to those observed for linear polyethylene prepared by a calendar molding process[13,14] and for poly(tetramethylene terephthalate) prepared by elongation of the amorphous film at several temperatures between 80 and 200 °C.[15] On the basis of our previous studies,[13-15] we conclude that these units correspond to single row-nucleated cylindrites or an assembly of them. The density in this film is almost constant during the formation of the rodlike textures from the isotropic medium, as shown in Figure 5. This would be expected if the extent of crystallinity of the hard segments is hardly affected by the elongation ratio.

Figure 6 shows the corresponding H_v light scattering patterns at various extension ratios. The scattering from the drawn specimens up to $\lambda = 1.2$ and 1.5 shows a broad four-leaf pattern while that from specimens drawn to $\lambda = 2.0$ and 3.0 shows the superposition of a broad-leaf pattern and a sharp pattern of streaks. The angle α that the H_v scattering lobes make with respect to the equator is apparently related to the angle that the optically anisotropic rodlike textures makes with respect to the stretching direction. The angle α is nearly 45°. Therefore, from the H_v scattering pattern, we can support the result of polarized micrographs for which the rods are oriented at around 45° with respect to the stretching direction. Sharp four-leaf streaks have sometimes been observed for oriented crystalline films such as tubular extended poly(1-

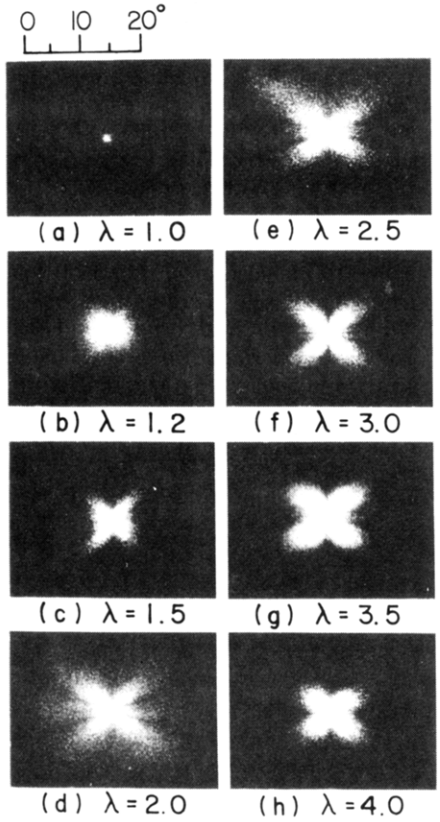

Figure 6. Change in H_v light scattering patterns of specimen P70B stretched at 120 °C.

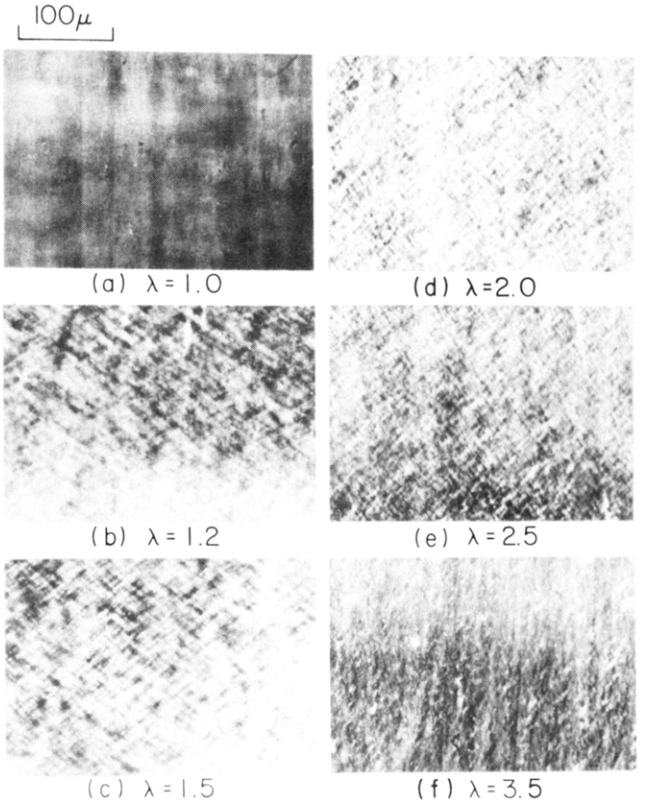

Figure 7. Polarized micrographs for poly(tetramethylene terephthalate) stretched at 120 °C.[15]

butene)[16] and poly(ethylene terephthalate).[17] The streaks in those cases have been attributed to scattering from assemblies of sheaves. Accordingly, we believe that the streaks reflect interparticle intereference effects from the rods.

In order to facilitate understanding of the above concept, we refer to published polarized micrographs and the corresponding small-angle light scattering patterns of drawn poly(tetramethylene terephthalate) homopolymer.[15] Figure 7 shows the polarized micrographs of the film stretched at 120 °C. The rods are oriented at a particular angle with respect to the stretching direction and form networks. The rod axes at $\lambda = 1.2$ were predominantly oriented perpendicular to the stretching direction rather than parallel. This indicates predominant growth of the rods in the direction perpendicular to the stretching direction. With further increase in elongation, the rods become oriented more and more in the stretching direction while preserving the network structure up to $\lambda = 4.0$ and the corresponding H_v scattering exhibits a sharp four-leaf pattern as streaks, as shown in Figure 8. By contrast, as shown in Figure 6, the sharp streaks disappeared when specimen P70B was stretched beyond $\lambda = 3.5$. This is due to the disappearance of the network structure in Figure 4.

Judging from the series of the micrographs and the corresponding H_v light scattering patterns, we believe that the streaks reflect an interparticle interference effect from the rods, as concluded in the case of scattering from the assembly of sheaflike textures. Accordingly, the angle γ that the sharp H_v scattering streaks make with respect to the equator is thought to be associated with an angle between the line connecting the center of the rods and the stretching direction, as shown in Figure 9. Patterns similar to Figure 9 appeared, for example, in the case of poly(tetramethylene terephthalate) stretched to $\lambda = 1.5$, as discussed in previous work. The white lines in the

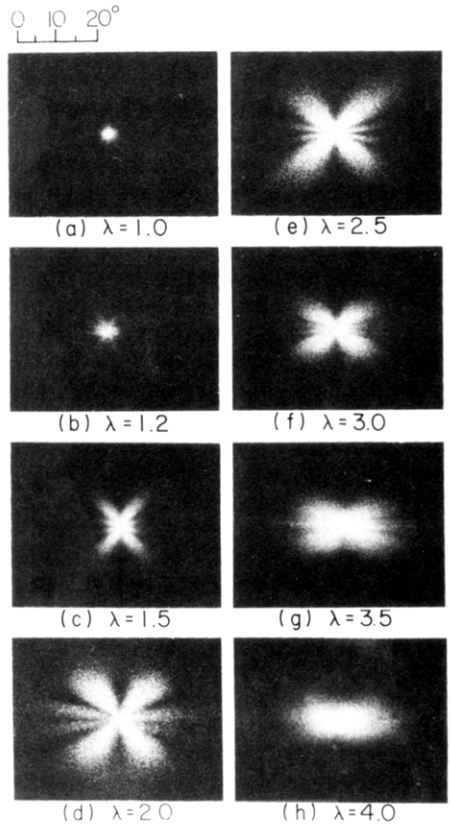

Figure 8. Change in H_v light scattering patterns for poly(tetramethylene terephthalate) stretched at 120 °C.[15]

polarizing micrograph d are drawn along assemblies of rods to make clear the interparticle interference effect. Actually, as shown in Figure 9, the angles α and γ are associated with an average orientation angle of the rods and that of their assembly, respectively, with respect to the stretching

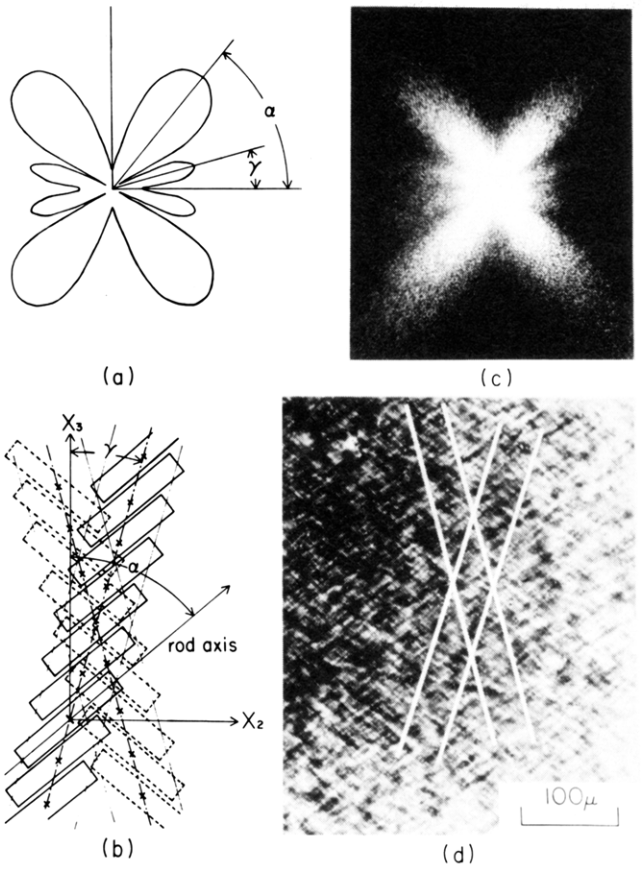

Figure 9. Schematic diagrams for H_v light scattering patterns and oriented rods:[15] (a) schematic representation of H_v light scattering pattern; (b) schematic representation of arrangement for rodlike textures with respect to the stretching direction; (c) H_v light scattering pattern observed at $\lambda = 1.5$; (d) polarized micrograph at $\lambda = 1.5$.

direction. Through the series of experiments on poly(tetramethylene terephthalate) and for this segmented polyether–polyester block copolymer, our schematic concept is confirmed as reasonable.

As for the V_v scattering from poly(tetramethylene oxide)–poly(tetramethylene terephthalate) block polymer and poly(tetramethylene terephthalate) homopolymer, the intensity distribution for all patterns caused no significant azimuthal dependence similar to the indistinct circular type in spite of the change of elongation ratio. Accordingly, these patterns are not shown. This is probably due to the fact that the difference of the polarizability perpendicular to the scattering element axis and the polarizability of the medium has a very large value, as pointed out by Moritani et al.[18] Unfortunately, it was impossible to analyze the morphological properties of these block polymers and homopolymers using such indistinct V_v scattering patterns.

In order to obtain more conclusive evidence, we refer to the model system shown in Figure 10 to calculate light scattering patterns theoretically. Efforts have been made to preserve the notation of Blundell[19,20] in order to emphasize the similarity of formulation between small-angle light and X-ray scattering. In this model system, the z_3 axis corresponds to the scattering direction and the X_3 axis is parallel to the direction of an incident beam whose unit vector is defined as $\mathbf{s}_0$. The intensity distribution is observed as a function of the scattering angle θ and the azimuthal angle μ, and $\mathbf{s}'$ is a unit vector along the scattered laser beam. In order to simplify the calculations, it is assumed that rods are rectangular in cross section and situated in the plane O–Y_3Z_3. The center of gravity of each

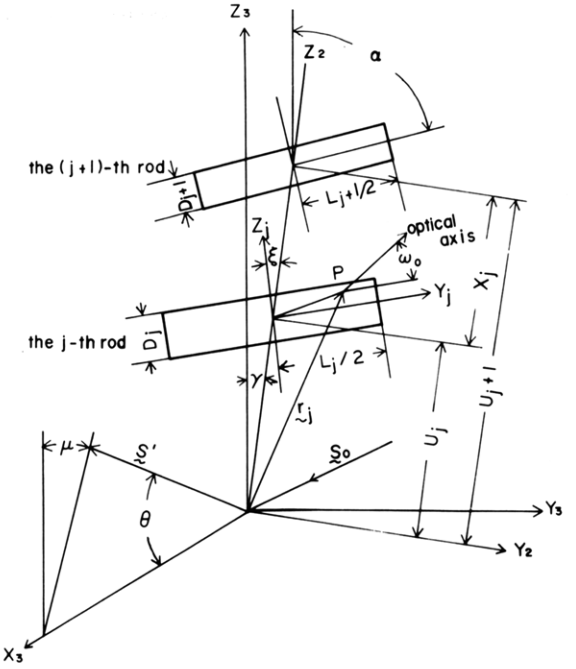

Figure 10. Model used for the theoretical analysis of the light scattering intensity distribution.

rod is in the direction of the Z_3 axis. As for the jth rod, the y_j and z_j axes are parallel and perpendicular, respectively, to the direction of the rod axis. The dimensions of the jth rod are represented by the length L_j and the width D_j, and ξ denotes the orientational angle between the z_j and Z_2 axes. In order to simplify the calculation, the angle γ is a constant value and ξ is given as a function of α. The optical axis is assumed to form a polar angle ω_0 with respect to the rod axis and to lie in a rectangular plane. The calculation was carried out for H_v scattering.

Considering the geometrical arrangement of the rods in Figure 10, the scattering amplitude from the jth rod whose center of gravity is situated at a distance u_j from the center of the coordinate system O–$Z_3Y_3X_3$ is given by

$$a_j(s) = \int_S \rho_0 \exp[-2\pi i(\mathbf{s}\cdot\mathbf{r}_j)]\, d\mathbf{S} \qquad (2)$$

where $\mathbf{s}$ is $(\mathbf{s}' - \mathbf{s}_0)/\lambda'$ and λ' is the wavelength in the medium. ρ_0 is the scattering power per unit area under H_v polarization conditions, which is given by

$$\rho_0 = \mathbf{M}\cdot\mathbf{O} = \frac{\delta_0}{2} \cos\rho_2 \sin\{2(\xi + \omega_0 - \gamma)\}E_0 \qquad (3)$$

where $\mathbf{M}\cdot\mathbf{O}$ denotes the scalar product of the induced dipole moment $\mathbf{M}$ and the vector $\mathbf{O}$ along the polarization direction of the analyzer for the horizontal polarization. E_0 is the amplitude of an incident beam. δ_0 is the anisotropy of the scattering element defined by $\alpha_\parallel - \alpha_\perp$, which is assumed to be uniaxially symmetrical with polarizabilities $\alpha_\parallel$ and $\alpha_\perp$ along and perpendicular to the optical axis, and $\cos\rho_2$, as defined by Clough et al.,[21] is given by

$$\cos\rho_2 = \cos\theta/(\cos^2\theta + \sin^2\theta\sin^2\mu)^{1/2} \qquad (4)$$

According to the method proposed by Blundell,[19] the normalized scattered intensity from an assembly of N rods is $\sum\sum a_i(s)a_j^*(s)/N$. $a^*(s)$ denotes the complex conjugate of $a(s)$. As the result

$$I = \frac{1}{N}\sum_{i=1}^{N}\sum_{j=1}^{N} a_i(s)a_j^*(s) = I_B - I_C \qquad (5)$$

where I_B and I_C are given by

$$I_B = \mathrm{Re}\left\{J - G^2 + \frac{1 + F_x}{1 - F_x}G^2\right\} \quad (6)$$

$$I_C = \mathrm{Re}\left\{\frac{2G^2F_x(1 - F_x^N)}{N(1 - F_x)^2}\right\} \quad (7)$$

where

$$J = \int_0^{2\pi}\int_{-\infty}^{\infty}\int_{-\infty}^{\infty} p(\xi)M(D_j)h(L_j)f_j^2\,\mathrm{d}D_j\,\mathrm{d}L_j\,\mathrm{d}\xi \Big/ \int_0^{2\pi} p(\xi)\,\mathrm{d}\xi \quad (8a)$$

$$G = \int_0^{2\pi}\int_{-\infty}^{\infty}\int_{-\infty}^{\infty} p(\xi)M(D_j)h(L_j)f_j\,\mathrm{d}D_j\,\mathrm{d}L_j\,\mathrm{d}\xi \Big/ \int_0^{2\pi} p(\xi)\,\mathrm{d}\xi \quad (8b)$$

$$F_x = \int_{-\infty}^{\infty} H(X_j)\exp(-2\pi i b X_j)\,\mathrm{d}X_j \quad (8c)$$

and

$$b = \sin\theta\cos\mu/\lambda' \quad (9)$$

Equations 6 and 7 are the same formulation given by Hosemann and Bagchi[22] in the case when the fluctuation of the domain thickness has no correlation with the statistics of the lattice. The term I_B is mainly responsible for the first and higher order diffraction peaks, and the term I_C gives the zero-order scatter. The term $J - G^2$ in eq 6 corresponds to diffuse scattering, and the term Re $\{(1 + F_x)/(1 - F_x)\}$ corresponds to the reciprocal lattice factor, which converges to unity as the scattering angle θ increases. The scattering amplitude f_j from the jth rod in eq 8a–c leads to

$$f_j = \frac{1}{2}\sin\{2(\xi + \omega_0 - \gamma)\} \times \frac{\sin[\pi L_j \sin\theta \sin(\mu + \xi - \gamma)/\lambda']}{\pi L_j \sin\theta \sin(\mu + \xi - \gamma)/\lambda'} \times \frac{\sin[\pi D_j \sin\theta \cos(\mu + \xi - \gamma)/\lambda']}{\pi D_j \sin\theta \cos(\mu + \xi - \gamma)/\lambda'} E_0\delta_0\cos\rho_2 \quad (10)$$

Following Blundell,[20] we assume that the variations of the lengths L_j, D_j, and X_j are independent of each other and are given by the following symmetric functions with the respective mean lengths $\bar{L}$, $\bar{D}$, and $\bar{X}$ and the standard deviations σ_l, σ_d, and σ_x; thus

$$h(L_j) = (2\pi)^{-1/2}\sigma_l^{-1}\exp[-(L_j - \bar{L})^2/2\sigma_l^2] \quad (11a)$$

$$M(D_j) = (2\pi)^{-1/2}\sigma_d^{-1}\exp[-(D_j - \bar{D})^2/2\sigma_d^2] \quad (11b)$$

and

$$H(X_j) = (2\pi)^{-1/2}\sigma_x^{-1}\exp[-(X_j - \bar{X})^2/2\sigma_x^2] \quad (11c)$$

Equations 11a and 11b are associated with the fluctuations in the dimensions of the rods; σ_l and σ_d are the parameters describing the degree of fluctuations in rod length and in rod width, respectively. When all rods are the same size, σ_l and σ_d are equal to zero. But the fluctuation increases with increasing σ_l and σ_d. If there are no fluctuations of the rod size and the orientation, the term $J - G^2$ in eq 6 becomes zero. Equation 11c is associated with the distance statistics introduced by Hosemann.[22] When $\sigma_x = 0$, the displacement between the two adjacent rods is the same distance and with increasing σ_x, the fluctuation of displacement increases.

Substituting eq 11a–c into eq 8a and 8c, J and G^2 can be obtained, which is given in Appendix.

In a real system, the position of the specimen sampled by the laser beam contains a distribution of the number of rods N. This concept must be introduced in order to smear out the many subsidiary maxima that appear at lower scattering angle. This has been taken into consideration by Hashimoto et al.,[23] who introduced a discrete symmetrical distribution of N with standard deviation $\sigma_N = 3$ in order to calculate small-angle X-ray[23] and light[16] scattering intensities. This distribution is written as

$$P(N) = \exp\left\{-\frac{(N - \bar{N})^2}{2\sigma_N^2}\right\} \Big/ \sum_{N=1}^{2\bar{N}-1}\exp\left\{-\frac{(N - \bar{N})^2}{2\sigma_N^2}\right\} \quad (12)$$

In the present work, we will assume the same type of distribution of N. Then, the average value of the term I_C is given by

$$\langle I_C\rangle_{av} = \sum_{N=1}^{2\bar{N}-1} I_C P(N) \quad (13)$$

In our subsequent calculations, we assume an average $\bar{N}$ of 10. To complete this theoretical analysis, we now discuss the function $p(\xi)$ that appears in eq 8a–c. $p(\xi)$ is a distribution function describing the orientation of rods with respect to the Z_2 axis. It is defined by

$$p(\xi) = \exp[-\sigma_\xi^2\sin^2(\xi - \xi_0)] \quad (14)$$

where σ_ξ is a parameter associated with the shape of $p(\xi)$ and $p(\xi)$ shows a sharp distribution with increasing σ_ξ.

According to the theoretical analysis, the scattered intensity depends upon the structural parameters ξ_0, γ, σ_x, σ_l, σ_d, σ_ξ, $\bar{L}/\lambda'$, $\bar{D}/\bar{L}$, and $\bar{X}/\bar{D}$. Before carrying out the numerical calculations to evaluate the scattered intensity, it should be noted that since the area of each rod is related to the absolute intensity but not to the profile of the intensity distribution function, the intensity in eq 5 was normalized by $(\rho_0\bar{L}\bar{D})^2$ to carry out the numerical calculation.

Let us consider the μ dependence of the scattered intensity distribution. Figure 11 shows the patterns calculated, in which the values of all parameters except γ, ξ_0, and σ_ξ are fixed. That is, the parameters describing the fluctuations in the rod length and width were set at very small values such as $\sigma_l/\bar{L} = \sigma_d/\bar{D} = 0.001$ and the parameter describing the fluctuation in identity period was fixed at $\sigma_x/\bar{X} = 0.5$, to simplify the analysis for the calculated patterns. The parameters associated with the sharpness of rods and their situation are fixed as $\bar{L}/\lambda' = 40$, $\bar{D}/\bar{L} = 0.05$, and $\bar{X}/\bar{D} = 40$, respectively, to avoid overlapping of neighboring rods even in the random orientation of rods. The parameter σ_ξ, denoting the orientational fluctuation of rods, was set as 2 and 100 to characterize two extremes of the distribution function $p(\xi)$, the former broad and the latter narrow. The parameter γ to determine the profile of the scattering streaks was fixed as ±10°, since most of the patterns in Figures 6 and 8 have the four-leaf streaks around μ = 80, 100, 260, and 280°, respectively. The parameter ξ_0 represented as $\pi/2 + \gamma - \alpha$ was calculated by using each value of the angle α estimated from the various scattering patterns observed. Incidentally, the value of α can be determined from the patterns observed by considering that eq A7 satisfies the μ dependence of the scattering lobes approximately except in the case of the random orientation of rods.

As illustrated in Figure 11, patterns a and b have four-leaf lobes at μ = 30, 150, 210, and 330°, respectively, in the case of $\xi_0 = \pm 40°$, patterns c and d at μ = 45, 135, 225, and 315°, respectively, in the case of $\xi_0 = \pm 55°$, and finally patterns e and f at μ = 55, 125, 235, and 305°,

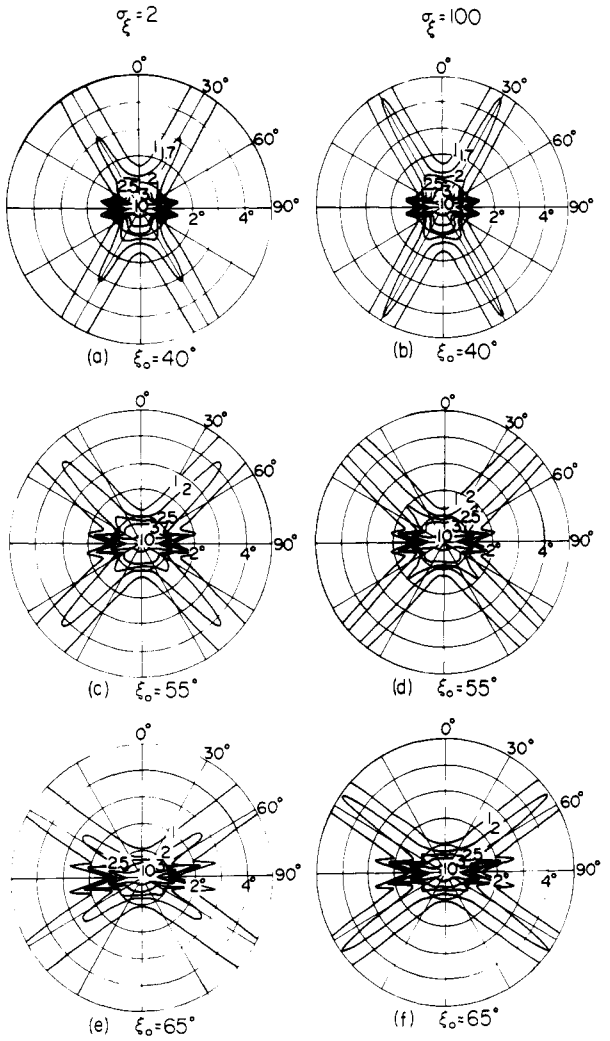

Figure 11. H_v light scattering patterns with change in ξ_0 and σ_ξ, in which the other parameters are fixed at $\sigma_l/\bar{L} = \sigma_d/\bar{D} = 0.001$, $\sigma_x/\bar{X} = 0.5$, $\bar{D}/\bar{L} = 0.05$, $\bar{X}/\bar{D} = 40$, $\bar{L}/\lambda' = 40$, and $\gamma = \pm 10°$ at small scattering angles up to 5°.

respectively, in the case of $\xi_0 = \pm 65°$. By contrast, all patterns have four-leaf streaks at $\mu = 80$, 100, 260, and 280°, respectively, by setting $\gamma = \pm 10°$. In the above condition, the angle α is almost equal to ±60° at $\xi_0 = \pm 40°$, equal to ±45° at $\xi_0 = \pm 55°$, and equal to ±35° at $\xi_0 = \pm 65°$, respectively, since ξ in eq A1 and A2 is close to ξ_0 ($= \pi/2 + \gamma - \alpha$) at $\sigma_\xi \geq 2$. That is, the profile of the scattering patterns indicates that eq A7 and A10 satisfy the μ dependence of lobes and streaks, respectively. Thus, it may be concluded that information concerning the orientation of rods and that of the assemblies may be obtained on the basis of the geometrical relation shown in Figure 9. Incidentally, the orientational fluctuation of rods reflects the profile of scattering lobes. An increase of σ_ξ, i.e., a decrease of the fluctuation, causes the scattering lobes to sharpen, as can be seen in the comparison between the patterns on the right and those on the left. This effect becomes considerable as the scattering angle θ increases, while the four-leaf streaks are hardly affected by the orientational fluctuations, because of the constant values of $\gamma = \pm 10°$.

Figure 12 shows the patterns calculated at $\xi_0 = 65°$ and $\sigma_\xi = 100$ to study the effect of the dimensional fluctuations of rods over wide scattering angles up to 10°. The numerical calculation was carried out by using the parameters $\sigma_x/\bar{X}$, $\sigma_l/\bar{L}$, and $\sigma_d/\bar{D}$, the values being different from those used to calculate the patterns in Figure 11. As can be seen in patterns a–d, the third-order peak of streaks appears at $\mu = 80°$ (or 100, or 260, or 280°) when $\sigma_l/\bar{L} = 0.001$ (or

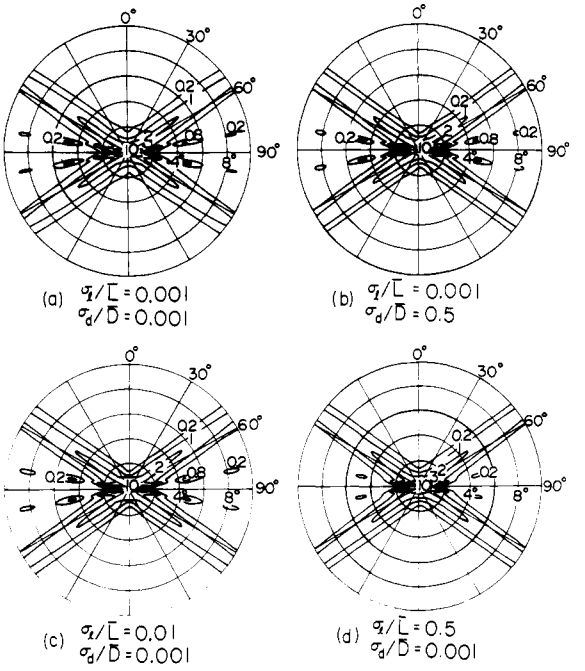

Figure 12. H_v light scattering patterns with change in $\sigma_l/\bar{L}$ and $\sigma_d/\bar{D}$, in which ξ_0 and σ_ξ are fixed at ±65° and 100, respectively, and the values of the other parameters are the same as used in Figure 11.

0.01), indicating small dimensional fluctuation in rod length, while it does not appear when $\sigma_l/\bar{L} = 0.5$, indicating the large fluctuation. By contrast, the peak is nearly independent of the value of $\sigma_d/\bar{D}$. This result indicates that the high order peak is affected by the fluctuation in rod length but is hardly affected by that in rod width. In addition, the fluctuation in rod length causes no significant change in the scattering lobes as does the fluctuation in the rod width.

IV. Conclusion

An interesting phenomenon has been found, namely, the appearance of rodlike textures in poly(tetramethylene oxide)–poly(tetramethylene terephthalate) block copolymer. This has been confirmed by polarizing microscopy. The rodlike textures were formed when the amorphous films with no deformation were preheated for 10 min at several temperatures between 80 and 160 °C and then stretched beyond an elongation ratio of $\lambda = 1.2$. Through the preheating process, no superstructure was observed in the specimen, but its elongation yields rodlike textures oriented at a particular angle around 45° with respect to the stretching direction. The rods formed networks at an elongation ratio less than $\lambda = 3.0$. With further elongation, the networks are disrupted but the rods are still oriented at around 45°. Although there is no orientation of the rods, the molecular chain axes of the soft and hard segments became oriented more and more in the stretching direction, which was measured by means of infrared dichroism and birefringence. The density of this specimen had almost a constant value during the formation of rodlike textures from isotropic medium.

On the basis of the above information, small-angle light scattering was used in order to analyze the orientation of rods and the network structures quantitatively. The scattering from the specimen that formed the network structures shows a superposition of a broad four-leaf pattern as lobes and a sharp four-leaf pattern as streaks. The angle α that the H_v scattering lobes make with respect to the equator was almost equal to the angle that the rods make with respect to the stretching direction. On the other

hand, the angle γ that H_v scattering streaks make with respect to the equator is almost equal to the angle that the assembly line connecting the center of the rods makes with respect to the stretching direction. Such relations were found in the drawn specimen of poly(tetramethylene terephthalate) homopolymer which was prepared by using a method similar to that used for segmented polyester P150B and P70B. In order to facilitate understanding of the above concept, the intensity distribution for the light scattering pattern was calculated by using the schematic diagram in Figure 10. With a proper choice of α and γ, the patterns calculated were in good agreement with those observed. This result supports the concept shown in Figure 9.

Acknowledgment. We thank Professor Kawai, Hyogo Education College, Japan, for valuable comments and suggestions. Thanks are due to Dr. Ishihara, Katada Institute, Toyo-bo Co., Ltd., for the sample used and for helpful comments.

Appendix

Substituting eq 11a–c into eq 8a–c, we obtain

$$J = (\bar{L}\bar{D}\delta_0 E_0 \cos^2 \rho_2/2)^2 \int_0^{2\pi} p(\xi) \sin^2 \{2(\xi + \omega_0 - \gamma)\} \times \{[1 - \cos \{2\pi\bar{L} \sin \theta \sin (\mu + \xi - \gamma)/\lambda'\} \times \exp\{-2\pi^2\sigma_l^2 \sin^2 \theta \sin^2 (\mu + \xi - \gamma)\}]/[\pi\bar{L} \sin \theta \sin (\mu + \xi - \gamma)/\lambda']^2\} \times \{[1 - \cos \{2\pi\bar{D} \sin \theta \cos (\mu + \xi - \gamma)/\lambda'\} \times \exp\{-2\pi^2\sigma_d^2 \sin^2 \theta \cos^2 (\mu + \xi - \gamma)\}]/[\pi\bar{D} \sin \theta \cos (\mu + \xi - \gamma)/\lambda']^2\} \, d\xi / \int_0^{2\pi} p(\xi) \, d\xi \quad \text{(A1)}$$

$$G = (\bar{L}\bar{D}\delta_0 E_0 \cos \rho_2/2) \int_0^{2\pi} p(\xi) \sin \{2(\xi + \omega_0 - \gamma)\} \times \frac{\sin \{\pi\bar{L} \sin \theta \sin (\mu + \xi - \gamma)/\lambda'\}}{\pi\bar{L} \sin \theta \sin (\mu + \xi - \gamma)/\lambda'} \times \exp\left[-\frac{1}{2}\pi^2\sigma_l^2 \sin^2 \theta \sin^2 (\mu + \xi - \gamma)/\lambda'^2\right] \times \frac{\sin \{\pi\bar{D} \sin \theta \cos (\mu + \xi - \gamma)/\lambda'\}}{\pi\bar{D} \sin \theta \cos (\mu + \xi - \gamma)/\lambda'} \times \exp\left[-\frac{1}{2}\pi^2\sigma_d^2 \sin^2 \theta \cos^2 (\mu + \xi - \gamma)/\lambda'^2\right] d\xi / \int_0^{2\pi} p(\xi) \, d\xi \quad \text{(A2)}$$

and

$$F_x = |F| \exp\{-2\pi i \sin \theta \cos (\mu - \gamma)\bar{x}/\lambda'\} \quad \text{(A3)}$$

where

$$|F| = \exp\{-2\pi^2 \sin^2 \theta \cos^2 (\mu - \gamma)\sigma_x^2/\lambda'^2\} \quad \text{(A4)}$$

The angle ω_0 is fixed as 0°.

If there is no orientational fluctuation of, i.e., $\xi = \xi_0$, ξ_0 becomes equivalent to $\pi/2 + \gamma - \alpha$. In addition to the above assumption, if all rods have the same size, i.e., $\sigma_l = \sigma_d = 0$, eq 12 and 13 are reduced to

$$J = (\bar{L}\bar{D}\delta_0 E_0 \cos^2 \rho_2/2)^2 \cos^2 \{2(\omega_0 - \alpha)\} \times \frac{\sin^2 \{\pi\bar{L} \sin \theta \sin (\mu - \alpha)/\lambda'\}}{\{\pi\bar{L} \sin \theta \sin (\mu - \alpha)/\lambda'\}^2} \times \frac{\sin^2 \{\pi\bar{D} \sin \theta \cos (\mu - \alpha)/\lambda'\}}{\{\pi\bar{D} \sin \theta \cos (\mu - \alpha)/\lambda'\}^2} \quad \text{(A5)}$$

and

$$G = (\bar{L}\bar{D}\delta_0 E_0 \cos \rho_2/2) \cos \{2(\omega_0 - \alpha)\} \times \frac{\sin \{\pi\bar{L} \sin \theta \sin (\mu - \alpha)/\lambda'\}}{\pi\bar{L} \sin \theta \sin (\mu - \alpha)/\lambda'} \times \frac{\sin \{\pi\bar{D} \sin \theta \cos (\mu - \alpha)/\lambda'\}}{\pi\bar{D} \sin \theta \cos (\mu - \alpha)/\lambda'} \quad \text{(A6)}$$

If $\bar{D} \to 0$, the term $\sin \{\pi\bar{D} \sin \theta \cos (\mu - \alpha)/\lambda'\}/\{\pi\bar{D} \sin \theta \cos (\mu - \alpha)/\lambda'\}$ in eq A6 becomes unity, and therefore G^2 has maximum value at $\mu = \alpha + \pi/2$ and $\alpha + 3\pi/2$. In a real system, we have to consider another condition $-\alpha$ to calculate the theoretical pattern. Accordingly, the azimuthal dependence of the scattered intensity exhibits a maximum value at the following angles:

$$\mu = \pi/2 + \alpha$$
$$\mu = 3\pi/2 + \alpha$$
$$\mu = \pi/2 - \alpha$$
$$\mu = 3\pi/2 - \alpha \quad \text{(A7)}$$

Returning to eq 6 and 7, we note that since we cannot define eq 6 and 7 at $F_x = 1$, the normalized scattered intensity must be obtained by using another simple analysis. The result is given by

$$I/N = J + (N - 1)G^2 \quad \text{(A8)}$$

where the coefficient $(N - 1)/2$ satisfies the condition

$$\mathrm{Re}\left\{\frac{1 + F_x}{1 - F_x} - \frac{2F_x(1 - F_x^N)}{N(1 - F_x)^2}\right\} \leq N \quad \text{(A9)}$$

Equation A9 indicates that the scattered intensity distribution has a maximum value at $F_x = 1$.

Considering eq A3 and A4, one can derive that F_x becomes unity both at $\mu - \gamma = \pi/2$ and $3\pi/2$. Since we must consider another condition $-\gamma$ in a real system, we can derive the following conditions:

$$\mu = \pi/2 + \gamma$$
$$\mu = 3\pi/2 + \gamma$$
$$\mu = \pi/2 - \gamma$$
$$\mu = 3\pi/2 - \gamma \quad \text{(A10)}$$

The relations represented as eq A7 and A10 are important in analyzing the profile of H_v scattered intensity distribution.

Registry No. (Terephthalic acid)·(polytetramethylene glycol)·(1,4-butanediol) (copolymer), 37282-12-5.

References and Notes

(1) Cooper, S. L.; Tobolsky, A. V. *J. Appl. Polym. Sci.* **1968**, *10*, 1837.
(2) Cella, R. J. *J. Polym. Sci., Part C* **1973**, *42*, 727.
(3) Kimura, I.; Ishihara, H.; Ono, H.; Yoshihara, N.; Nomura, S.; Kawai, H. *Macromolecules* **1974**, *7*, 355.
(4) Schen, M.; Mehra, U.; Niinomi, M.; Koberstein, J. T.; Cooper, S. L. *J. Appl. Phys.* **1974**, *45*, 4182.
(5) Seymour, R. W.; Overton, J. R.; Corley, L. S. *Macromolecules* **1975**, *8*, 331.
(6) Lilaonitkul, A.; West, J. C.; Cooper, S. L. *J. Macromol. Sci., Phys.* **1976**, *B12*, 563.
(7) Inoue, T.; Soen, T.; Kawai, H.; Fukatsu, M.; Kurata, M. *J. Polym. Sci., Part B* **1968**, *6*, 75.
(8) Matsuo, M.; Sagu, S.; Asai, H. *Polymer* **1969**, *10*, 79.
(9) Inoue, T.; Soen, T.; Hashimoto, T.; Kawai, H. *J. Polym. Sci., Part A-2* **1969**, *7*, 1283.
(10) Inoue, T.; Soen, T.; Hashimoto, T.; Kawai, H. *Macromolecules* **1970**, *3*, 87.
(11) Matsuo, M.; Geshi, K.; Moriyama, A.; Sawatari, C. *Macromolecules* **1982**, *15*, 193.
(12) Stein, R. S.; Misra, A. *J. Polym. Sci.* **1980**, *18*, 327.
(13) Hashimoto, T.; Nagatoshi, K.; Kawai, H. *Polymer* **1976**, *17*, 1075.

(14) Matsuo, M.; Ozaki, F.; Sugawara, S.; Ogita, T. *Macromolecules* **1980**, *13*, 1187.
(15) Sawatari, C.; Muranaka, T.; Matsuo, M. *Polym. J.* **1983**, *15*, 33.
(16) Hashimoto, T.; Todo, A.; Kawai, H. *Polym. J.* **1978**, *10*, 521.
(17) Matsuo, M.; Tamada, M.; Terada, T.; Sawatari, C.; Niwa, M. *Macromolecules* **1982**, *15*, 985.
(18) Moritani, M.; Hayashi, N.; Utsuo, A.; Kawai, H. *Polym. J.* **1971**, *2*, 74.
(19) Blundell, D. J. *Acta Crystallogr., Sect. A* **1970**, *A26*, 472.
(20) Blundell, D. J. *Acta Crystallogr., Sect. A* **1970**, *A26*, 476.
(21) Clough, S.; van Aartsen, J. J.; Stein, R. S. *J. Appl. Phys.* **1965**, *36*, 3072.
(22) Hosemann, R.; Bagchi, S. N. "Direct Analysis of Diffraction by Matter"; North-Holland Publishing Co.: Amsterdam, 1962.
(23) Hashimoto, T.; Nagatoshi, K.; Todo, A.; Hasegawa, H.; Kawai, H. *Macromolecules* **1974**, *7*, 264.

Poly(α-amino acids) Carrying Amphiphilic Side Chains. Synthesis, Conformation, Hydrophobic Binding, and Induced Circular Dichroism

Masahiko Sisido,*† Keiji Akiyama,‡ and Yukio Imanishi‡

Research Center for Medical Polymers and Biomaterials and Department of Polymer Chemistry, Kyoto University, Kyoto 606, Japan. *Received July 7, 1983*

ABSTRACT: Poly(L- and D-glutamine) derivatives carrying hydrophobic groups and quaternized amino groups were prepared. Their circular dichroism indicated the charged-coil conformation in water. The formation of hydrophobic clusters in aqueous solution was evidenced by enhanced excimer formation of 4-(1-pyrenyl)butyric acid in the presence of the amphiphilic poly(α-amino acids). The efficiency of hydrophobic binding by the amphiphilic polymer was much higher than that by low molecular weight detergents and similar to that by quaternized laurylpoly(ethylenimine). Induced circular dichroism was observed when certain cyanine dyes were adsorbed onto the amphiphilic poly(α-amino acids). However, no circular dichroism or circularly polarized fluorescence was detected when chromophores or fluorophores less bulky than the cyanine dyes were mixed with the amphiphilic poly(α-amino acids). It was therefore concluded that the amphiphilic poly(α-amino acids) provide a hydrophobic environment that is achiral in a local region but chiral in a spatially extended region.

Structures and functions of molecular assemblies of amphiphilic substances in water are of current interest in membrane-mimetic chemistry.[1] Polymers may play an important role in this field, since the main chain may stabilize the assembly structures, which are otherwise unstable physically and chemically. Attempts have been reported recently to reinforce the bilayer structure by a polymeric framework.[2-5] Polymers carrying amphiphilic side chains have been reported previously.[6,7] For example, quaternized laurylpoly(ethylenimine) (I) was shown to bind

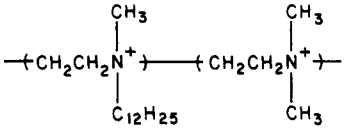

I

hydrophobic molecules effectively in aqueous solution.[8] This polymer detergent was found to have the following advantages over low molecular weight detergents. First, smaller amounts of amphiphilic groups are required to bind a given amount of hydrophobic substrate than in the case of low molecular weight detergents. This property of polymer detergents leads to a higher effective concentration of substrate taken up in the hydrophobic cluster. Second, the amphiphilic polymer forms micelle-like clusters even at the lowest concentration examined (10^{-6} M with respect to the lauryl group). This means that the polymer detergent has virtually no critical concentration at which the hydrophobic cluster begins to appear. Third, the amphiphilic polymer can be recovered by ultrafiltration, which is especially important from a practical point of view.

Since the main chain of poly(ethylenimine) is highly branched and has a randomly coiled conformation, the hydrophobic cluster should have no ordered structure. In order to develop novel amphiphilic assemblies that have a regular and chiral structure, we have undertaken a synthesis of poly(α-amino acids) carrying amphiphilic side chains. In this article, the syntheses of poly(L- and D-glutamine) derivatives having cationic side chains (II) and amphiphilic side chains (III) are described. The hydrophobic binding of a pyrenyl chromophore by these polymers was examined on the basis of the excimer formation, and the chirality of the polymeric cluster was studied by the induced circular dichroism of cyanine dyes adsorbed onto the cluster.

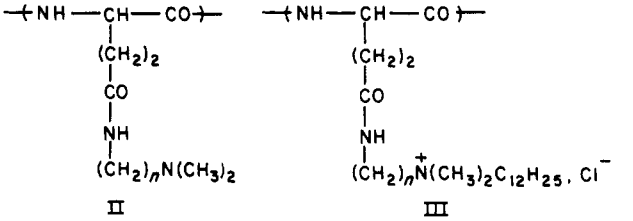

II

L-3 ($n = 3$, L isomer)
D-3 ($n = 3$, D isomer)
L-6 ($n = 6$, L isomer)

III

L-3-12 ($n = 3$, L isomer)
D-3-12 ($n = 3$, D isomer)
L-6-12 ($n = 6$, L isomer)

Besides the general advantages of polymeric detergents mentioned above, the amphiphilic poly(α-amino acids) are expected to show the following characteristics. First, the chiral and possibly helical polypeptide main chain may provide a novel amphiphilic structure with a high degree of ordering and chirality, which one may utilize as a medium for stereospecific reactions and interactions. Second,

† Research Center for Medical Polymers and Biomaterials.
‡ Department of Polymer Chemistry.

0024-9297/84/2217-1773$01.50/0